Available online at www.sciencedirect.com

SciVerse ScienceDirect

Ceramics International 39 (2013) 6751–6762

CERAMICS INTERNATIONAL

www.elsevier.com/locate/ceramint

Dissolution properties of different compositions of biphasic calcium phosphate bimodal porous ceramics following immersion in simulated body fluid solution

Yin Zhang[a,b,*], Jianan Ai[a], Dinggai Wang[a], Zhongrong Hong[a], Wenhui Li[a], Yoshiyuki Yokogawa[c]

[a]*Nanjing University of Technology, No. 5 Xinmofan Road, Nanjing, 210009, China*
[b]*Nanjiang Haoqi Advanced Materials Co., Ltd, Gaochun Economic Development Zone, Nanjing, China*
[c]*Osaka City University, 3-3-138 Sugimoto-cho, Sumiyoshi-ku, Osaka, 558-8585, Japan*

Received 3 October 2012; received in revised form 2 February 2013; accepted 2 February 2013
Available online 16 February 2013

Abstract

Biphasic calcium phosphate (BCP) bimodal porous ceramics were prepared from a mixture of fine powders of hydroxyapatite (HAp) and beta-tricalcium phosphate (β-TCP) with varying HAp/β-TCP ratios. Two types of HAp powders and one type of β-TCP powder were used to produce porous BCP bioceramics with HAp/β-TCP weight ratios of 20/80, 40/60, and 80/20. Dissolution tests were performed to compare the dissolution properties of BCP-based bioceramics with different structural properties. Porous ceramic samples of approximately 0.5 g were individually soaked in 30 ml of simulated body fluid (SBF) solution at 36.5 °C for 1, 3, 7 and 10 days, respectively. The calcium content of the SBF solution was analyzed by ICP. The porous bodies were filtered, dried, and characterized using SEM, XRD, and FT-IR. The results indicate that the sample structural properties seem to have a greater effect than the storage environment on the dissolution properties.

Keywords: Biphasic calcium phosphate; Bimodal porous ceramics; Dissolution; SBF

1. Introduction

A scaffold with acceptable biocompatibility is one of the key factors required for successful tissue engineering leading to tissue regeneration [1]. Tissue engineering is a rapidly developing area that requires the use of biodegradable and biocompatible scaffolds as three-dimensional supports for initial cell attachment and subsequent tissue organization, formation and growth [2]. Bone substitutes should possess the following desirable physical and biochemical properties: (1) interconnected porosity, (2) biodegradability, (3) bioactivity, (4) osteoconductivity and (5) osteoinductivity [3,4]; thus, in recent years, attention has been directed to the development of resorbable and osteoinductive biomaterials from calcium phosphates [5,6–10]. In the case of CaP bioceramics, interconnected porosity can be engineered to a certain extent [4,11–13] or can be derived from natural materials of biologic origin (e.g., corals and bovine bone) [4,14–17].

The most widely used calcium phosphate-based bioceramics are hydroxyapatite [HA, $Ca_{10}(PO_4)_6(OH)_2$] and β-tricalcium phosphate [β-TCP, $Ca_3(PO_4)_2$]. HAp is stable in body fluid, while TCP is soluble [18]. The in vivo and in vitro dissolution of calcium phosphate ceramics depends on the composition and crystallinity of the ceramic and on the pH of the solution [19–22]. However, many studies have indicated that the dissolution of HAp in the human body after implantation is too low to achieve optimal results. Conversely, the dissolution rate of β-TCP ceramics is too fast for bone bonding. To achieve an optimum resorbability of the material, studies have mainly focused on the biphasic calcium phosphate ceramics composed of

*Corresponding author at: Nanjing University of Technology, No. 5 Xinmofan Road, Nanjing, 210009, China. Tel.: +86 25 83587787.
E-mail address: zhangyin512@gmail.com (Y. Zhang).

0272-8842/$ - see front matter © 2013 Elsevier Ltd and Techna Group S.r.l. All rights reserved.
http://dx.doi.org/10.1016/j.ceramint.2013.02.004

HA and TCP [23–25]. Several studies have suggested that the resorbability of biphasic ceramics is largely determined by the HAp/TCP ratio [26]. However, the particle properties and porosity influence the dissolution rate and affect the material–tissue interaction [27]. Therefore, it is necessary to produce biphasic ceramics with various HAp/TCP ratios in a simple and systematic way. Furthermore, the mechanisms controlling dissolution require further investigation.

This study reports the preparation of high porosity bimodal biphasic calcium phosphate (BCP) ceramics with different particles of HAp and β-TCP and characterizes the dissolution behavior of the resulting materials. Therefore, the investigation of the dissolution mechanisms of calcium phosphates immersed in simulated body fluid (SBF) solution provides relevant information about the mechanism of precipitation of the bone-like calcium phosphate layer.

2. Materials and methods

A commercial HAp (HAp2) powder (Taihei chemical Co., Ltd) was used as-received and HAp (HAp1) and β-TCP powders were synthesized in the laboratory for the production of bimodal type porous BCP ceramics. The two different HAp powders have different particle sizes and specific surface areas. HAp1 and β-TCP composite powders were synthesized by mechanochemical methods using calcium hydrogen phosphate di-hydrate ($CaHPO_4 \cdot 2H_2O$) and calcium carbonate ($CaCO_3$). The details of the powder synthesis have been described elsewhere [28].

Six different batches of HAp/ β-TCP (BCP) powders were prepared as follows:

Mixtures of the pure laboratory synthesized HAp1 and β-TCP powders at weight ratios of 20/80 HAp1/β-TCP (BCP1-1), 40/60 HAp1/β-TCP (BCP1-2) and 80/20 HAp1/β-TCP (BCP1-3) were added at 65.0 wt% to water to make slurries. Mixtures of the commercial pure HAp2 powder and the pure laboratory-synthesized β-TCP powder were prepared at weight ratios of 20/80 HAp2/β-TCP (BCP2-1), 40/60 HAp2/β-TCP (BCP2-2) and 80/20 HAp2/β-TCP (BCP2-3) and added at 65.0 wt% to water to make slurries. The slurry was mechanically agitated at room temperature for 2 h. The reacted slurry was then dried in air at 60 °C for 7 days and heat-treated in air at 750 °C for 8 h to produce a fine BCP powder. The processing parameters for each batch are shown in Table 1, which shows different particle sizes and specific surface areas. The six batches of powders were used to produce bimodal type porous BCP ceramics.

A slip was obtained by adding BCP powders to a solution of 1.5% deflocculant and 0.5 wt% foaming agent. The optimum value of the minimum viscosity in these BCP slips with respect to the solid loading and the optimum amount of the deflocculant were investigated. The specimen obtained by casting a 0.5 wt% polyurethane foam (medium pore size type supplied by Ube Industries Inc.) into a slip and drying under vacuum at 60 °C was heated at 1150 °C for 3 h. Approximately 0.5 g of the obtained porous ceramic samples were soaked in 30 ml of simulated body fluid (SBF) solution at 36.5 °C for 1, 3, 7 and 10 days. Similar to a concentrated form of simulated body fluid (SBF), by a biomimetic process adapted from the work of Kokubo et al. [29,30]. A bone-like layer formed on BCP, which was reported to be poorly crystallized carbonated apatite [31,32], was observed by a scanning electron microscope (SEM). The porous body was dried and characterized using SEM, XRD and FT-IR.

Table 1
Particle sizes and specific surface areas of the HAp1, HAp2, β-TCP and BCP powders.

Powder	Particle size (μm)	Specific surface area (m^2/g)	HAp/ β-TCP	Viscosity (mpas)	Shear stress (pas)	pH of slip
HAp1	0.34	38.01	–	–	–	–
HAp2	2.84	3.81	–	–	–	–
β-TCP	0.70	20.04	–	–	–	–
BCP1-1	0.49	28.56	20/80	474.90	4.84	8.57
BCP2-1	1.06	17.18	20/80	323.93	3.30	8.61
BCP1-2	0.54	24.46	40/60	427.91	4.36	8.46
BCP2-2	1.41	14.94	40/60	226.95	2.31	8.27
BCP1-3	0.44	35.74	80/20	665.86	6.79	8.18
BCP2-3	2.13	9.11	80/20	277.94	2.83	7.65

The weight changes were calculated by comparing the dry weight (W_s) of the sample after immersion for a predetermined time with the original dry weight (W_o) of the sample according to the equation

$$\text{Weight change}(\%) = (W_s - W_o)/W_o \times 100\%$$

The average particle diameter of the synthesized powder was measured using a centrifugal sedimentation method with a 0.2% solution of sodium pyrophosphate as a dispersion medium and using SA-CP3 from the Shimadzu Co. The specific surface area was measured using the BET method. The crystal phase of the synthesized powder and sintered powders were each examined by an X-ray powder diffraction method using an X-ray diffractometer at 40 KV and 20 mA with CuKa radiation (wavelength = 1.54056 Å) (MAC Science, MXP3). Identification of the phases was achieved by comparing the diffraction patterns with ICDD (JCPDS) standards. A fourier transform infrared (FT-IR) analysis (Jasco, MFT-2000) using KBr was also done. The densities of the porous BCP bodies were obtained by the water immersion method based on the Archimedean principle (the average value of five samples). All densities were as a percentage of the theoretical density of HAp of 3.156 g/cm^3 and TCP of 3.18 g/cm^3. The Ca^{2+} concentration change of the samples after immersion in a SBF solution was determined (the average value of three samples, per porous ceramic samples of approximately

0.5 g) by ICP (Seiko, ISM7000s). Scanning electron microscopy (SEM) and EDX analysis of the powders and sintered body were performed using a Hitachi S-3000, and a Horiba EMAX-2200 X-ray analyzer. The pore size distribution was measured using mercury intrusion porosimetry (AutoPore-9500 of Shimadzu Co.).

3. Results and discussion

3.1. Powder characterization

The ICP-derived Ca/P molar ratios of the HAp1, HAp2 and β-TCP powders were 1.67 ± 0.01, 1.67 ± 0.03 and 1.51 ± 0.01, respectively. XRD analysis showed that HAp1, HAp2 (ICDD 09-0432) and β-TCP (ICDD 09-0169) only exhibited peaks corresponding to HAp and β-TCP [33]. This was further evidence that the materials in this study were single-phase HAp and single-phase β-TCP that did not decompose to secondary phases on sintering/heating. The particle size and specific surface areas of the three powders are listed in Table 1. Fig. 1 shows SEM photos of the HAp1, HAp2 and β-TCP powders. The laboratory-synthesized HAp1 and β-TCP powders exhibited round shapes with nodular projections. The commercial HAp2 powders were hexagonal length rods.

The XRD patterns of the BCP powders before exposure to SBF solution were identified as the BCP phase, as shows in Fig. 2. The peaks in XRD were sharp, indicating the high crystalline order of the material. All the apatite peaks corresponding to ICDD 09-0432 and the β-TCP peaks corresponding to ICDD 09-0169 were present in the spectrum and no additional peaks of any other calcium phosphates were seen. It could be concluded that the whole mass was existing in double phases. Moreover, the peak height ratio of HAp and β-TCP was dependent of HAp size. This means that the powders were homogeneously mixed and there was little contamination during ball milling. This is evidence that the material created in this study was double-phased on sintering/heating. The synthesized BCP powders produced a diffraction pattern that corresponded to a crystalline material, with narrow diffraction peaks characteristic of a powder that has been heat-treated in air at 750 °C for 8 h.

The morphologies of the six powders were illustrated in the SEM micrographs shows in Fig. 3. The BCP1-1 particle was round with nodular projections. BCP1-1 and BCP2-1 particles were the same, only the BCP2-1 particles were slightly elongated. The BCP1-2 and BCP2-2 particle shapes are nearly the same, with the exception that the BCP2-2 particles were slightly thicker. The BCP1-3 and BCP2-3 particle shapes were significantly different. Because HAp2 accounts for 80% of BCP2-3, many different particle shapes are observed in this sample; in addition, these particles are shorter and thicker than HAp2 particles.

Although the chemical and phase compositions of the three groups of powders are similar, their characteristics, including size distribution, surface area and morphology are quite different. These differences must be due to the differences in the primary powders of HAp1 and HAp2. The particle parameters for each batch are presented in Table 1.

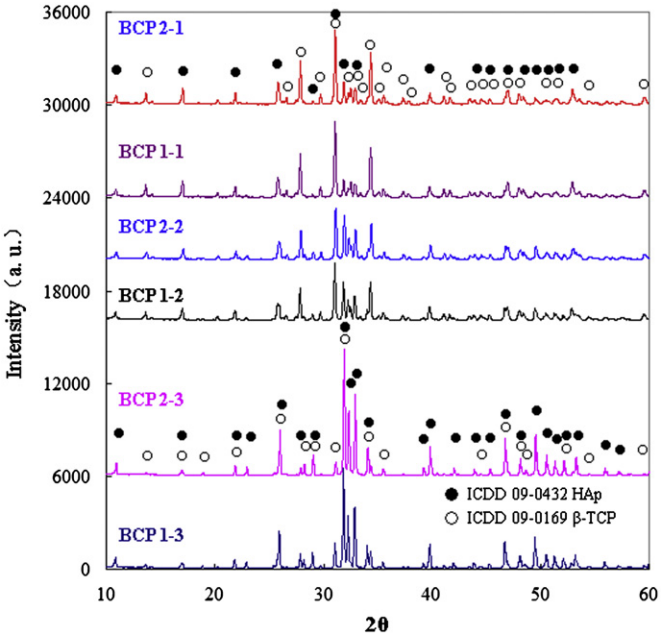

Fig. 2. XRD patterns of BCP1-1 and BCP2-1, BCP1-2 and BCP2-2, BCP1-3 and BCP2-3 powders by heating at 750 °C for 8 h.

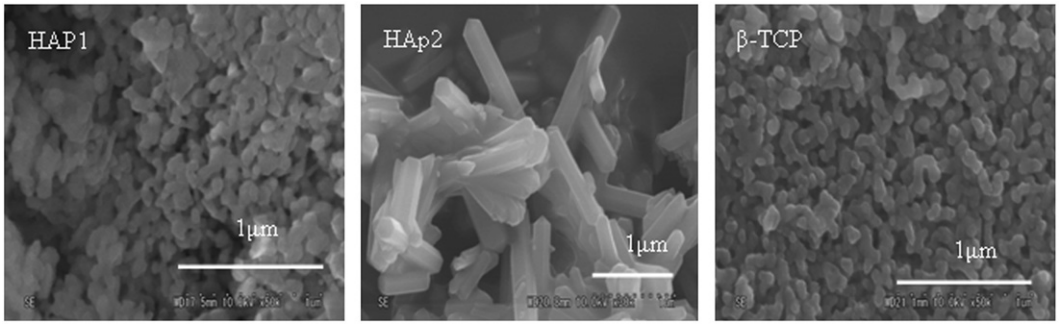

Fig. 1. SEM photos of HAp1, HAp2 and β-TCP powders.

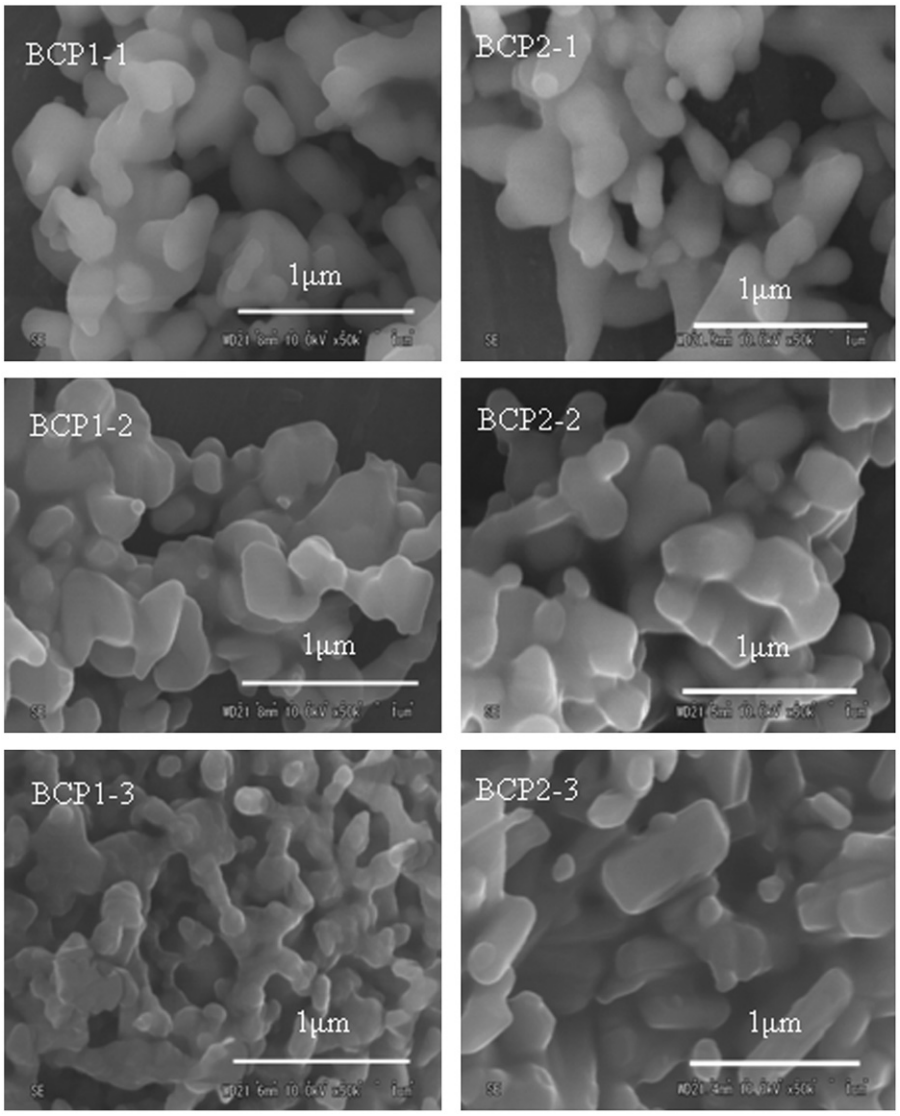

Fig. 3. SEM photos of BCP1-1 and BCP2-1, BCP1-2 and BCP2-2, BCP1-3 and BCP2-3 powders by heating at 750 °C for 8 h.

3.2. Slip characterization and foaming

Particle size and powder concentration greatly influence the rheological behavior of slurries [34]. To obtain a BCP slurry with a reasonably low viscosity for solid loading, BCP1-1, BCP1-2, BCP1-3, BCP2-1, BCP2-2 and BCP2-3 powder concentrations were all 65.0 wt%, with 1.5 wt% dispersant. The viscosity and shear stress of the six slurries are showed in Table 1. The viscosity of the slurries containing 65.0 wt% powder showed similar behaviors versus deflocculant concentration. The shear stress of slurries prepared with BCP1-1, BCP1-2 and BCP1-3 powders, which have larger specific surface areas, was larger than that of the BCP2-1, BCP2-2 and BCP2-3 powders. Similarly, the viscosity of the slurry prepared with the BCP1-1, BCP1-2 and BCP1-3 powders, which have larger specific surface areas, was larger than that of the BCP2-1, BCP2-2 and BCP2-3 powders, which have smaller specific surface areas. The optimum solid loading to achieve the minimum viscosity in the present BCP1-1, BCP1-2, BCP1-3, BCP2-1, BCP2-2 and BCP2-3 slips were all 65.0 wt%. The specimen obtained by dipping a 0.5 wt% polyurethane foam into a slip and drying it under vacuum was heated at 1150 °C for 3 h. The purpose of the heat-treatment process was to remove volatiles and the urethane foam to form a porous network.

3.3. Pore structure

For the BCP sintered body obtained by heating at 1150 °C for 3 h, the foam with 1.5 wt% deflocculant and 0.5 wt% foaming reagent was dipped in the slips. The numbers of micropores for the specimens obtained from BCP1-1, BCP1-2 and BCP1-3 were larger than those of samples BCP2-1, BCP2-2 and BCP2-3, respectively. However, the sizes of the macropores from BCP2-1, BCP2-2 and BCP2-3 were larger than those for the samples BCP1-1, BCP1-2 and BCP1-3, respectively. SEM observation reveals that BCP foams were typically composed of large spherical pores with small

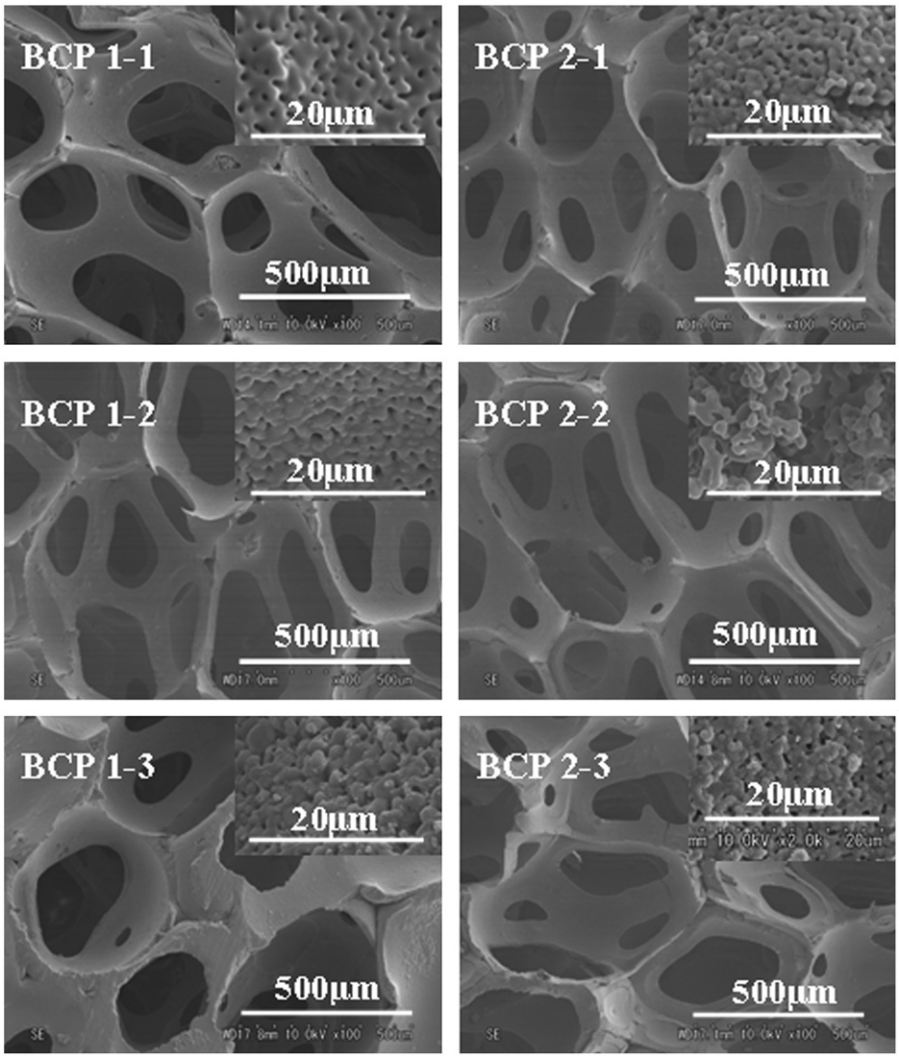

Fig. 4. SEM photos of BCP1-1, BCP2-1, BCP1-2, BCP2-2, BCP1-3 and BCP2-3 porous body by heating at 1150 °C for 3 h.

interconnecting rectangular pores, as shows in Fig. 4. The large spherical pore size is approximately 300 μm. A large number of small pores were observed distributed around the walls of the large spherical pores, generally in the size range of 0.1–10 μm. These pores appear to be highly interconnected, as confirmed by mercury porosimetry, as shows in Fig. 5. A large number of small pores in the size range of several μm or smaller were observed in the specimen obtained from the BCP sintered body obtained by heating at 1150 °C for 3 h (the foam was dipped in the BCP slip with 1.5 wt% of deflocculant and 0.5 wt% of foaming reagent), and these small pores could have formed due to the addition of the surfactant. Table 2 presents the particle parameters for the six different bimodal BCP porous ceramic sintered bodies.

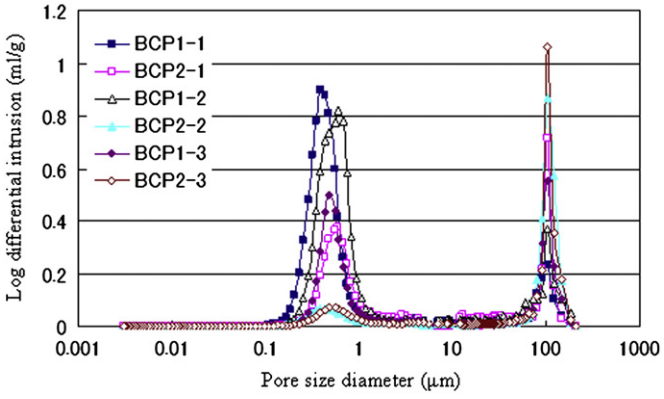

Fig. 5. Pore size distribution of bimodal porous BCP ceramics scaffolds prepared heated at 1150 °C for 3 h.

3.4. Dissolution properties

Table 2 presents the characteristics of the six different types of BCP ceramic sintered bodies. Fig. 6 shows the Ca^{2+} concentration in the SBF solution as a function of immersion time for the sintered body samples of BCP1-1 and BCP2-1, BCP1-2 and BCP2-2, and BCP1-3 and BCP2-3. Note that the increases in Ca^{2+} concentration in supersaturation were greater for BCP1-1 than for

Table 2
Characteristics of the six kind different bimodal BCP porous ceramics sintered body.

Powder	HAp/β-TCP	Porosity (%)	Relative density (%)
BCP1-1	20/80	59.03	31.07
BCP2-1	20/80	61.46	28.65
BCP1-2	40/60	61.72	29.72
BCP2-2	40/60	70.46	21.42
BCP1-3	80/20	56.70	34.77
BCP2-3	80/20	77.38	11.05

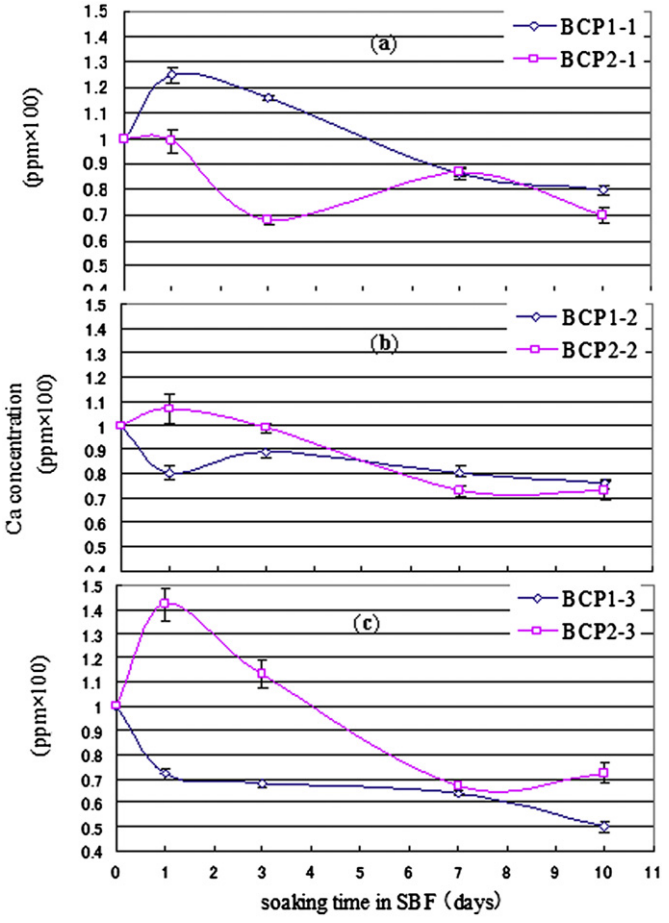

Fig. 6. The Ca^{2+} concentration change of the samples after immersion in a SBF solution as a function of soaking time.

BCP2-1, for BCP2-2 than for BCP1-2, and for BCP2-3 than for BCP1-3.

For the BCP1-1 and BCP2-1 sintered bodies from Fig. 6(a), during the first step (0–1 days), an increase in Ca^{2+} concentration was observed, indicating that the dissolution of BCP may have surpassed the new phase formation. The new phase deposited on the BCP surface was apatite. This result was proved by SEM, XRD patterns and FT-IR spectrum, as shown in Figs. 7–10 Note that the increase in Ca^{2+} concentration in supersaturation for BCP1-1 sintered body is greater than that for BCP2-1 sintered body. The new phase formed more rapidly on the surface of the BCP1-1 sintered body than on the surface of the BCP2-1 sintered body. The ion uptake takes place after this initial dissolution. It is apparent in Fig. 6(a) that the rates of precipitation during the first step (0–1 days) were in the order of BCP1-1 > BCP2-1. During the second step (1–3 days), a decrease in Ca^{2+} concentration was measured, indicating that formation of the new phase on the surface of the BCP1-1 and BCP2-1 ceramics may have surpassed dissolution. The new phase formation occurs more rapidly for BCP1-1 than for BCP2-1. During the third step (3–7 days), these samples exhibit different dissolution behavior. BCP1-1 continued to form the new phase, while BCP2-1 changed to dissolution. During the fourth step (7–10 days), BCP2-1 changed to form a new phase. For BCP1-1, the curve become flat. The two dissolution processes tend towards a kinetic equilibrium.

The dissolution behaviors of the BCP1-2 and BCP2-2 sintered bodies reported in Fig. 6(b) are different during the first step (0–1 days). BCP1-2 exhibited a rapid reduction in Ca^{2+} concentration in supersaturation, followed by a slow increase in Ca^{2+} concentration in supersaturation. Three days later the curve became more stable, with the dissolution processes tending towards a kinetic equilibrium. The dissolution behavior of BCP2-2 was similar to that of BCP1-1. The only difference was the Ca^{2+} concentrations in supersaturation. For BCP2-2, after 7 days the precipitation rate of the new phosphate increases, equilibrating the Ca^{2+} dissolution.

The BCP1-3 and BCP2-3 sintered bodies from Fig. 6(c) exhibited significantly different dissolution behaviors during the entire process. For BCP1-3, during the first step (0–1 days), a rapid reduction in Ca^{2+} concentration occurred in supersaturation. The dissolution processes tend toward a kinetic equilibrium one day later. Then, the Ca^{2+} concentration in supersaturation slowly decreases 7 days later. BCP2-3 showed a rapid increase in Ca^{2+} concentration during the first step (0–1 days), indicating that dissolution of BCP may have surpassed the new phase formation. Then, the Ca^{2+} concentration in supersaturation rapidly decreased, followed by a slow increase over the course of days 1–7. The new phase (apatite) deposited on the BCP1-3 and BCP2-3 surface was less than BCP1-1, BCP1-2, BCP2-1 and BCP2-2, as shown in Figs. 7 and 8.

The dissolution properties of the six different types of BCP ceramic sintered bodies soaked in SBF solution at 36.5 °C for 1, 3, 7 and 10 days were significantly different. The results demonstrate that the dissolution behavior was highly dependent on the composition, surface properties and scaffold construction. The result was correspondent with the SEM photograph. The new phase (apatite) deposited on the BCP surface are shown in Figs. 7 and 8.

Based on the above results, the micropores appear to exert the greatest influence on dissolution. For example, differences in microporosity could account for differences in the dissolution behaviors of BCP1-1 and BCP2-1 sintered bodies, which had nearly identical composition

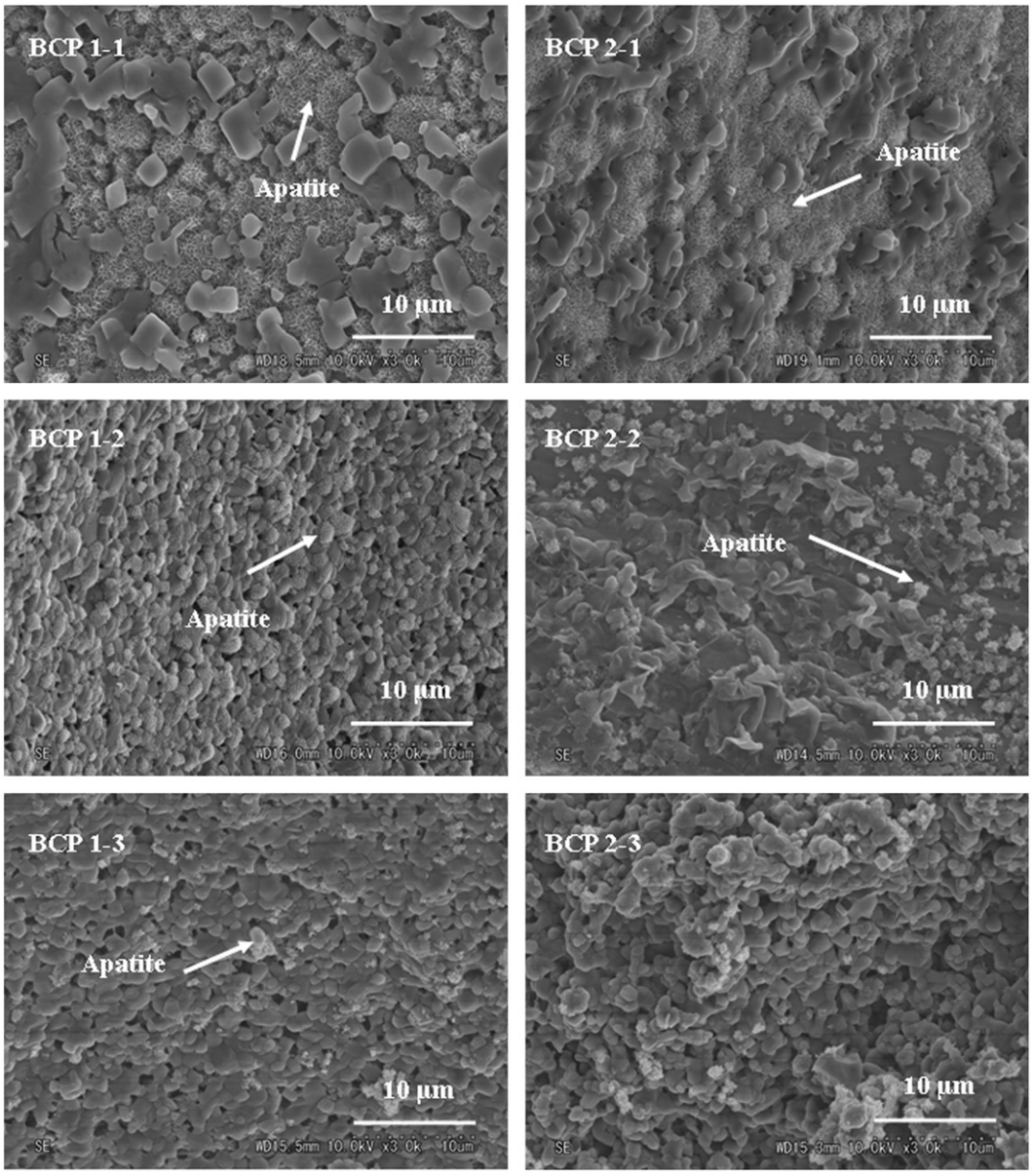

Fig. 7. SEM photograph showing the surface morphology of the BCP1-1, BCP1-2, BCP1-3, BCP2-1, BCP2-2 and BCP2-3 sintered body in SBF solution for 1 day.

and porosity. When porosity and composition are varied, porosity appears to have a greater influence on dissolution.

3.5. Morphology of the reacted surface

Figs. 7 and 8 present the surfaces of the BCP1-1 and BCP2-1, BCP1-2 and BCP2-2, and BCP1-3 and BCP2-3 sintered bodies after immersion in SBF solution for 1 day and one week, respectively. These images demonstrate clear differences in the morphologies of these surfaces. The apatite on BCP surface immersed in SBF solution for 1 day are small in amount and minute in form than 7 days. For the 7 days BCP samples, the BCP1-1, BCP2-1, BCP1-2 and BCP2-2 sintered bodies were fully converted to spherulitic shapes with an average diameter of 1.0–5.0 μm. The surfaces of the spherulites exhibit fine, needle-like structures. For the BCP1-3 and BCP2-3 sintered bodies after one week of immersion in SBF solution, a layer of precipitation was observed under high magnification, which was shown to be an amorphous or poorly crystallized new phase.

Based on the above results, the in vitro behavior of BCP sintered bodies was strongly affected by their composition, particle size, crystal structure, surface properties, porosity and scaffold construction.

The BCP1-1 versus BCP2-1 and BCP1-2 versus BCP2-2 sintered bodies have the same respective compositions, with BCP1-1 and BCP2-1 consisting of 20/80 HAp/β-TCP and BCP1-2 and BCP 2-2 consisting of 40/60 HAp/β-TCP. The β-TCP phase was the main component for each of these samples. The dissolution rate of β-TCP ceramics was

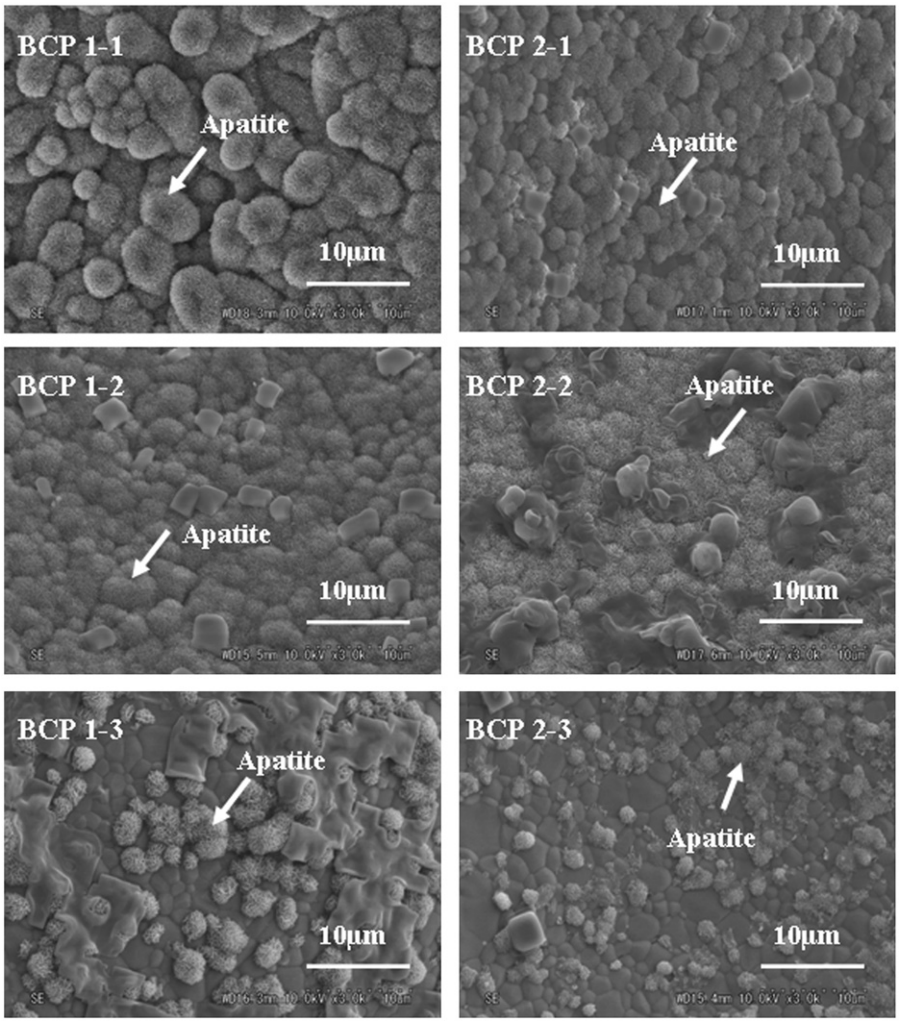

Fig. 8. SEM photograph showing the surface morphology of the BCP1-1, BCP1-2, BCP1-3, BCP2-1, BCP2-2 and BCP2-3 sintered body in SBF solution for one week.

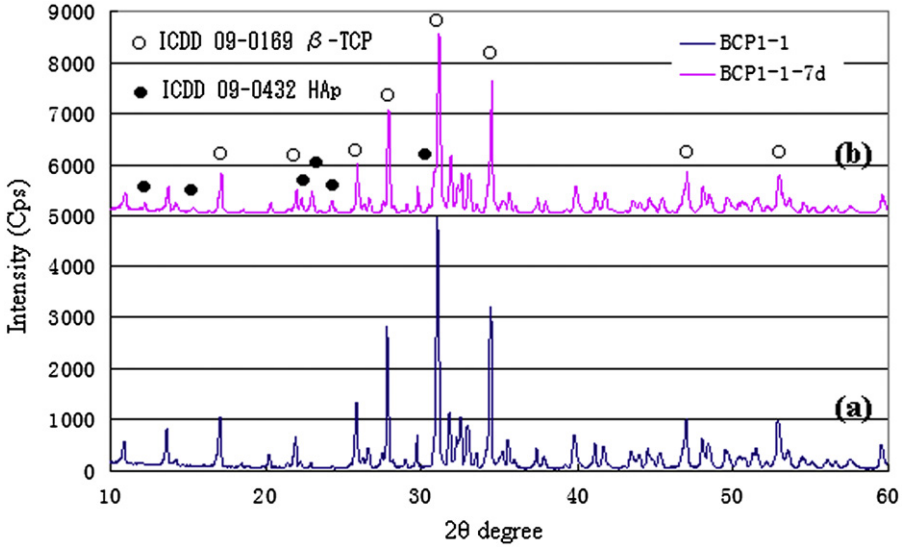

Fig. 9. XRD patterns of BCP1-1 porous body soaked in SBF various time periods. (a) 0 day and (b) 7 days.

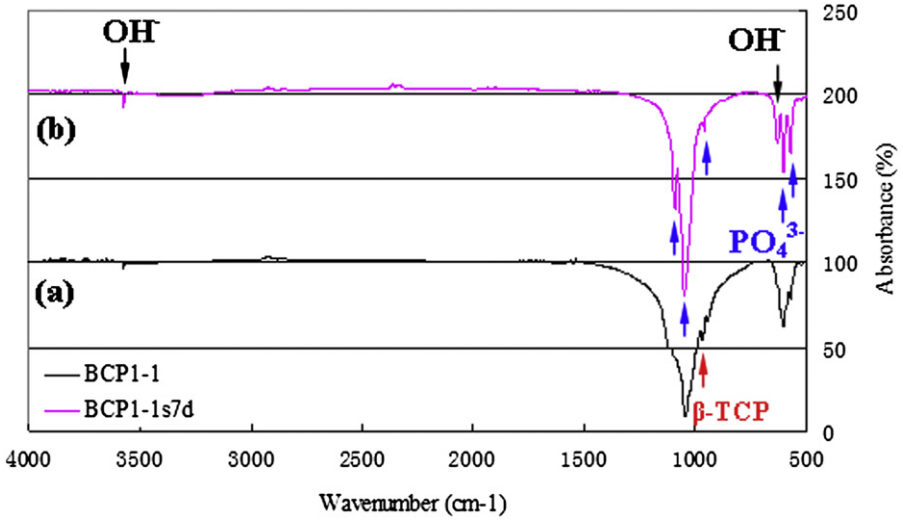

Fig. 10. FT-IR spectrum of BCP1-1 porous body soaked in SBF various time periods. (a) 0 day and (b) 7 days. Characteristic bands of HAp (571, 603, 632, 962, 1050, 1089 cm^{-1}) and the bands of β-TCP (972 cm^{-1}) can be observed.

faster than that of HAp ceramics. The BCP1-1, BCP2-1, BCP1-2 and BCP2-2 sintered bodies all formed needle shapes on the surface because these surfaces dissolved easily. The needles on the BCP1-1 and BCP2-1 ceramic surfaces were thicker than those on the BCP1-2 and BCP2-2 ceramics. These differences could result from the greater β-TCP content in BCP1-1 and BCP2-1 ceramics compared with BCP1-2 and BCP2-2 ceramics.

The BCP1-3 and BCP2-3 sintered bodes consisted of 80/20 HAp/β-TCP, with the HAp phase representing the major component of these samples. The dissolution rate of HAp ceramics was slower than that of β-TCP ceramics. BCP1-3 and BCP2-3 ceramics exhibited slow dissolution indicating that Ca^{2+} precipitation may have surpassed the new phase formation. A layer of precipitation was observed under high magnification and was shown to be an amorphous or poorly crystallized new phase on the surface of BCP1-3 and BCP2-3 sintered bodes.

3.6. The precipitated phase

The BCP1-1 porous body soaked in SBF with various time periods (i.e., the dried precipitate) had been subjected to phase and composition analysis (BCP1-1 porous body as a representative, the other basically consistent). The diffractogram is shown in Fig. 9 and the FT-IR spectrum in the wave number range 4000–500 cm^{-1} is shown in Fig. 10. Comparing the XRD patterns (Fig. 9a and b) of soaked in SBF with various time periods, it was seen that the new phases (apatite) form when BCP1-1 soaked in SBF for 7 days. And that β-TCP peak was decreased intensity. It was shown the β-TCP had a dissolving.

The FT-IR spectrum (Fig. 10a and b) contains the characteristic peaks due to OH^- group of apatite, around 3571 cm^{-1} and 632 cm^{-1}. The triply degenerated asymmetric stretching modes at 1089 cm^{-1} and 1050 cm^{-1} are the P–O bonds. The triply degenerated bending mode at 571 cm^{-1}, 603 cm^{-1} and 962 cm^{-1} are the O–P–O bonds. It is to be noted that typical HPO_4^{2-} peaks (at 1145 cm^{-1}, 1074 cm^{-1}, and 1022 cm^{-1}) in crystalline HAp are either not resolved or missing in the spectrum [35,36]. This means, the phosphate in the material is not well organized as crystal to form HPO_4^{2-} in the lattice. Comparing the curve of Fig. 10(a) and (b), the curve (b) of soaked in SBF for 7 days, it is characteristic band of HAp (571, 603, 632, 962, 1050, 1089 cm^{-1}) are stronger than the curve (a) of non soaked in SBF. However, the band of β-TCP (972 cm^{-1}) at Fig. 10(b) is missing. It means, the β-TCP on the surface of BCP porous body soaked in SBF for 7 days is dissolved, and the new HAp is formed on the surface of BCP porous body soaked in SBF for 7 days.

3.7. Weight changes

Fig. 11 shows the weight changes of the samples after immersion in SBF solution. Samples of the BCP1-2, BCP2-2 and BCP1-3 sintered bodies have an obvious tendency to increase in weight during the entire process. In contrast, samples BCP1-1, BCP 2-1 and BCP2-3 only significantly decrease in weight after 7 days. The weight changes of six types of samples were significantly different. Samples BCP1-1 and BCP 2-1 had the same porosity and composition but different initial particles (HAp1 versus HAp2, as shows in Table 1). The particle size of HAp1 was smaller and the BCP1-1 body was easily sintered, so it contained fewer micropores. Therefore, new phase formation on the surface of the BCP1-1 ceramics may have surpassed dissolution. The BCP2-1 sample was made from HAp2, which had a larger particle size, and the BCP2-1 body was difficult to sinter, leading to a high number of micropores in BCP2-1. Therefore, during the initial dissolution stage

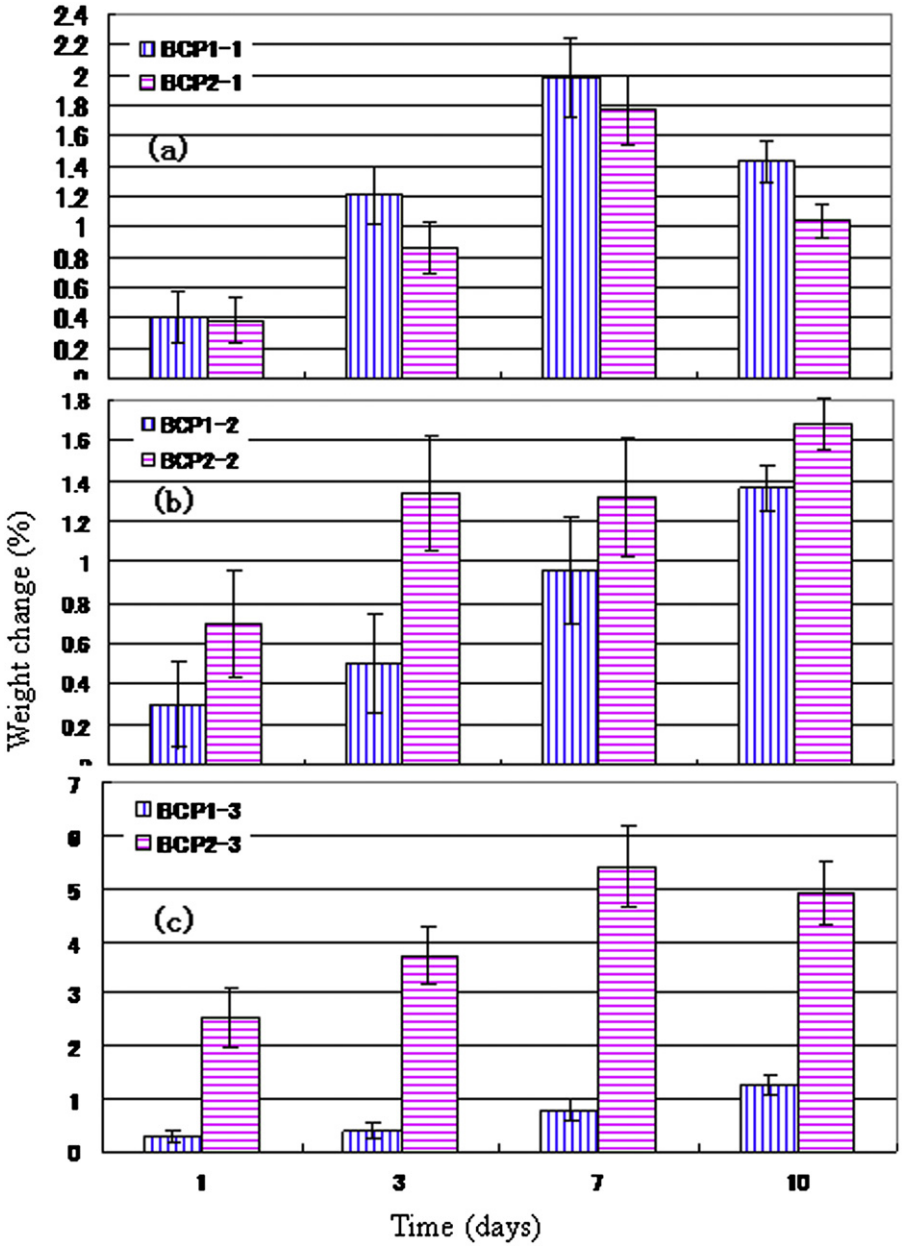

Fig. 11. The weight change of the samples after immersion in a SBF solution as a function of soaking time.

the dissolution on the surface of the BCP1-1 ceramics may have surpassed the new phase formation.

Fig. 11(a) shows that the weight increase on the surface of the BCP1-1 sintered body was larger than that of the BCP2-1 sintered body. When a new dissolution equilibrium was achieved, the change in weight tends to decrease, resulting in consistent dissolution properties.

The samples of BCP1-2 versus BCP2-2 or BCP1-3 versus BCP2-3 sintered bodies had the same composition but were prepared from different initial particles (HAp1 versus HAp2), resulting in significant differences in porosity, scaffold construction and weight change. The weight increases on the surfaces of BCP2-2 and BCP2-3 were larger than those on BCP1-2 and BCP1-3. This is consistent with the porosities of these samples, with BCP2-2 and BCP2-3 exhibiting greater porosities than BCP1-2 and BCP1-3. These results indicate that dissolution behavior was highly dependent on the porosity. Surfaces with greater porosities were expected to exhibit more precipitation than less porous surfaces. It is apparent in Fig. 11(b) and (c) that the rates of precipitation were in the order BCP2-3 > BCP2-2 > BCP1-2 > BCP1-3, consistent with the rank order of porosity. It is apparent in Table 2 that the rates of porosity were in the order BCP2-3 (77.38%) > BCP2-2 (70.46%) > BCP1-2 (61.72%) > BCP1-3 (56.70%).

The above results (such as the results of the BCP2-2 and BCP2-3 sintered bodies, which had porosities above 70%) suggest that highly porous samples exhibit rapid

dissolution during the initial stage and also more surface precipitation.

4. Summary

High porosity bimodal porous BCP ceramics were prepared from three powders by sintering at 1150 °C for 3 h. The ability of the sintered body to promote the precipitation of new calcium phases after soaking in SBF solution is directly related to its composition. This study showed that resorbability decreases with increasing HAp, with the rate of the reaction in proportion to the β-TCP content. Compositions with high β-TCP content can easily generate a new phase, and the resulting BCP1-1, BCP2-1, BCP1-2 and BCP2-2 bimodal porous ceramics showed high resorbability. The dissolution results confirmed that the biodegradation of calcium phosphate ceramics could be controlled by simply adjusting the amount of HAp or β-TCP in the bimodal porous BCP ceramics. The information gained from this research will provide a useful platform for further study.

Acknowledgments

A Project Funded by the Priority Academic Program Development of Jiangsu Higher Education Institutions.

References

[1] A. Haroun, Amira Gamal-Eldeen, R.K. David, Harding, Preparation, characterization and in vitro biological study of biomimetic three-dimensional gelatin–montmorillonite/cellulose scaffold for tissue engineering, Journal of Materials Science: Materials in Medicine 20 (2009) 2527–2540.

[2] J.P. Zheng, C.Z. Wang, K.D. Yao, Preparation of biomimetic three-dimensional gelatin/montmorillonite-chitosan scaffold for tissue engineering, Reactive and Functional Polymers 67 (2007) 780–788.

[3] R.Z. LeGeros, G. Daculsi, J.P. LeGeros, Bioactive Bioceramics, in: W.S. Pietrzak (Ed.), Musculoskeletal Tissue Regeneration, Biological Materials and Methods, Humana Press, Totowa, NJ, 2008, pp. 53–81.

[4] Sang-Jin Pankaj Sarin, D. Lee, Apostolov, M. Kriven, Porous biphasic calcium phosphate scaffolds from cuttlefish bone, Journal of the American Ceramic Society 94 (8) (2011) 2362–2370.

[5] J.O. Hollinger, J. Brekke, E. Gruskin, D. Lee, Role of bone substitute, Clinical Orthopaedics and Related Research 324 (1996) 55–66.

[6] H. Ohgushi, M. Okumura, T. Yoshikawa, T. Senpuku, K. Inoue, S. Tamai, E.C. Shors, Bone formation processin porous calcium carbonate and hydroxyapatite, Journal of Biomedical Materials Research 26 (1992) 885–895.

[7] Y. Yamazaki, S. Oida, Y. Akimoto, S. Shioda, Response of the mouse femoral muscle to an implant of a composite of bone morphogenetic protein and plaster of Paris, Clinical Orthopaedics and Related Research 234 (1988) 240–249.

[8] M.R. Urist, Lietze Arthur, Dawson Edgar, β-tricalcium phosphate delivery system for bone morphogenetic protein, Clinical Orthopaedics and Related Research 187 (1984) 277–280.

[9] G. Hotz, G. Herr, Bone substitute with. osteoinductive biomaterials-current and future. clinical applications, International Journal of Oral & Maxillofacial Surgery 23 (1994) 413.

[10] H.P. Yuan, J.D. De Bruijn, Y.B. Li, J.Q. Feng, Z.J. Yang, K. De Groot, X.D. Zhang, Bone formation induced by calcium phosphate ceramics in soft tissue of dogs: a comparative study between porous α-TCP and β-TCP, Journal of Materials Science-Materials in Medicine 12 (1) (2001) 7–13.

[11] T. Dutta Roy, J.L. Simon, J.L. Ricci, E.D. Rekow, V.P. Thompson, J.R. Parsons, Performance of degradable composite bone repair products made via three-dimensional fabrication techniques, Journal of Biomedical Materials Research Part A 66 (2) (2003) 283–291.

[12] S.H. Kwon, Y.K. Jun, S.H. Hong, I.S. Lee, H.E. Kim, Y.Y. Won, Calcium phosphate bioceramics with various porosities and dissolution rates, Journal of the American Ceramic Society 85 (12) (2002) 3129–3131.

[13] L. Muller, F.A. Muller, J. Zeschky, T. Fey, P. Greil, Fabrication of hydroxyapatite ceramics with interconnected macro porosity, Key Engineering Materials 284–286 (2005) 277–280.

[14] C. Demers, C. Reggie Hamdy, K. Corsi, F. Chellat, M. Tabrizian, L. Yahia, Natural coral exoskeleton as a bone graft substitute: a review, Bio-Medical Materials and Engineering 12 (1) (2002) 15–35.

[15] R.A. White, J.N. Weber, E.W. White, Replamineform: A new process for preparing porous ceramic, metal, and polymer prosthetic materials, Science 176 (4037) (1972) 922–924.

[16] S. Joschek, B. Nies, R. Krotz, A. Gopferich, Chemical and physicochemical characterization of porous hydroxyapatite ceramics made of natural bone, Biomaterials 21 (16) (2000) 1645–1658.

[17] R. Emadi, S.I. Roohani Esfahani, F. Tavangarian, A novel, low tem-perature method for the preparation of b-TCP/HAP biphasic nanostructured ceramic scaffold from natural cancellous bone, Materials Letters 64 (8) (2010) 993–996.

[18] L.L. Hench, J. Wilson., An Introduction to Bioceramics, World Scientific, London, UK, 1993.

[19] C.P.A.T. Klein, A.A. Driessen, K.d. Groot, V.D. Hoof, Biodegradation behavior of various calcium phosphate materials in bone tissue, The Journal of Biomedical Materials Research 17 (5) (1983) 769–784.

[20] A. Takeishi, H. Hayashi, H. Kamatsubara, A. Yokoyama, M. Kohri, T. Kawasaki, K. Miki, T. Kohgo, Implant of calcium phosphate ceramics altering Ca/P ratio in bone, Journal of Dental Research 68 (1989) 680–684.

[21] P. Ducheyne, S. Radin, L. King, The effect of calcium phosphate ceramic composition and structure on in vitro behavior. I. Dissolution, Journal of Biomedical Materials Research 27 (1993) 25–34.

[22] S.R. adin, P. Ducheyne, The effect of calcium phosphate ceramic composition and structure on in vitro behavior. II. Precipitation, Journal of Biomedical Materials Research 27 (1993) 35–45.

[23] M. Kohri, K. Miki, D.E. Waite, H. Nakajima, T. Okabe, In vitro stability of biphasic calcium phosphate ceramics, Journal of Biomaterials 14 (4) (1993) 299–304.

[24] N. Kivrak, A.C. TAS, Synthesis of calcium hydroxyapatite-tricalcium phosphate (HA-TCP) composite bioceramic powders and their sintering behavior, Journal of The American Ceramic Society 81 (1998) 2245–2252.

[25] X. Yang, Z. Wang, Synthesis of biphasic ceramics of hydroxyapatite and b-tricalcium phosphate with controlled phase content and porosity, Journal of Materials Chemistry 8 (1998) 2233–2237.

[26] Youn-Ki Soon-Ho Kwon, Seong-Hyeon Jun, Hyoun-He Kim Hong, Synthesis and dissolution behavior of β-TCP and HA/β-TCP composite powders, Journal of the European Ceramic Society 23 (2003) 1039–1045.

[27] Y. Zhang, Y. Yokogawa, T. Kameyama, Synthesis of apatite ceramics with bimodal pore structure using mechanochemically prepared fine apatite powder, Journal of Key Engineering Materials 280–283 (2005) 1571–1574.

[28] Y. Zhang, Y. Yokogawa, T. Kameyama, Influence of powder particle size of slurries on mechanical properties of porous hydroxyapatite ceramics, Journal of Key Engineering Materials 284–286 (2005) 365.

[29] T. Kokubo, H. Kushitani, S. Sakka, T. Kitsiugi, T. Yamamura, Solution able to reproduce in vivo surface-structure changes in

bioactive glass ceramics A–W, Journal of Biomedical Materials Research 24 (1990) 721–734.
[30] D.H. Barnes, R.E. Cameron, S. Kiamil, F. Meyer, R.A. Brooks, N. Rushton, S.M. Best, Biomimetic calcium phosphate coatings for polymeric artificial spinal disc implants, Journal of Bioceramics Development and Applications 1 (2011) ID D101111, 4 pp.
[31] A. Stoch, W. Jastrzebski, A. Brozek, B. Trybalska, M. Cichocinska, E. Szarawara, FTIR monitoring of the growth of the carbonate containing apatite layers from simulated and natural body fluids, Journal of Molecular Structure 511–512 (23) (1999) 287–294.
[32] Y. Yasuda, Mitsuhiro Aoki, Yohei Fujita, Wataru Fujitani, Yukichi Umakoshi, Akio Takaoka, Effect of β-TCP size on bone-like layer growth and adhesion of osteoblast-like cells in hydroxyapatite/β-TCP composites, Journal of Materials Transactions 47 (9) (2006) 2368–2372.
[33] PDF Card no. 09-0432 and 09-0169. ICDD, Newton Square, Pennsylvania, USA.
[34] T. Kokubo, H. Takadama, How useful is SBF in predicting in vivo bone bioactivity? Journal of Biomaterials 27 (2006) 2907–2915.
[35] S. Koutsopoulos, Synthesis and characterization of hydroxyapatit crystals: a review study on the analytical methods, Journal of Biomedical Materials Research 62 (2002) 600–612.
[36] S. Sureshbabu, Manoj Komath, H.K. Varma, In situ formation of hydroxyapatite-αlpha tricalcium phosphate biphasic ceramics with higher strength and bioactivity, Journal of the American Ceramic Society 95 (3) (2012) 915–924.